electronics

MDPI

Article

Hybrid Development of a Compact Antenna Based on a Novel Skin-Matched Ceramic Composite for Body Fat Measurement

Siamak Sarjoghian [1], Ardavan Rahimian [2,*], Yasir Alfadhl [1], Theo G. Saunders [3], Jiamin Liu [1] and Clive G. Parini [1]

[1] School of Electronic Engineering and Computer Science, Queen Mary University of London, London E1 4NS, UK; s.sarjoghian@qmul.ac.uk (S.S.); yasir.alfadhl@qmul.ac.uk (Y.A.); jiamin.liu@qmul.ac.uk (J.L.); c.g.parini@qmul.ac.uk (C.G.P.)

[2] School of Engineering, Ulster University, Newtownabbey BT37 0QB, UK

[3] School of Engineering and Materials Science, Queen Mary University of London, London E1 4NS, UK; t.g.saunders@qmul.ac.uk

* Correspondence: a.rahimian@ulster.ac.uk

Received: 8 November 2020; Accepted: 12 December 2020; Published: 14 December 2020

Abstract: This work presents the thorough hybrid (numerical and experimental) development of a miniaturized microwave antenna, to be better matched to the permittivity of the human skin. This would allow the abdominal fat to be measured more accurately, based on the employed reflection methods with minimal mismatches. This objective was achieved by designing the pyramidal horn antenna that was modeled based on the proposed and manufactured ceramic composite material. Moreover, by using the developed composite of barium titanate and titanium oxide, the ratio of the two could be precisely adjusted, so that the permittivity was a reasonable match to that of the skin. This step was validated by the open-ended probe method. This framework can be instrumental in a range of microwave biomedical applications, which aim to realize the body-centric systems.

Keywords: abdomen; antenna; biomedical system; body fat; ceramic; characterization; composite; double-ridged horn; high-dielectric material; microwave device; wideband

1. Introduction

Obesity and overweight are currently considered as the global risk factors to public health, resulting in the fast growth of cardiovascular diseases, diabetes, stroke, and other health-related consequences. A recent study has shown that global obesity will reach 18% in men, and 21% in women by 2025 [1].

The early diagnosis of fat accumulation in the human body, especially around the abdomen area, is important to prevent the growth of related diseases. The upsurge of the fat inside the body may result in the unwanted fat deposition, predominantly around the abdomen, hips, thighs, and other internal organs. Recent works have shown that abdominal fat results in higher health risks compared to the other types [2,3]. This is mainly due to the fact that abdominal fat is associated with other types of adipose tissues, accumulating around, as well as within the internal organs, such as the heart and kidneys [4].

Hence, accurate measurement of fat deposition in the body can be of great assistance to health services, plastic surgery, liposuction, and cosmetic procedures [5]. Moreover, general practitioners and dietitians rely on measuring waist size, to determine fat percentage in the abdominal cavity, using the body mass index (BMI) [6,7]. Though, this method is susceptible to human errors, and also lacks essential accuracy. To reduce errors, a number of standardized solutions have been used, such as

magnetic resonance imaging (MRI), computed tomography (CT), and ultrasound scan [8–13]. Several innovative methods have also been reported for microwave imaging purposes, as well as for biomedical detection and scanning [14,15].

As another method to precisely measure abdominal fat, ultra-wideband (UWB) methods can be mentioned. UWB refers to a specific frequency range (i.e., 3.1–10.6 GHz), and for the unlicensed use of this band, the signal strength must be less than a certain threshold (i.e., −41.3 dBm/MHz) [16]. The term wideband (WB) was introduced to refer to the pulses with a minimum bandwidth of 500 MHz, which can be either within or outside the standard UWB frequency range.

Furthermore, the pyramidal double-ridged horn (PDRH) antenna was designed in 1964 [17,18], though the ridged-waveguide was introduced earlier in 1947 [19]. This antenna is widely used in radar systems, due to its wide bandwidth, high gain, and high directivity. Due to its characteristics, this antenna is an efficient solution compared to the other bidirectional types, e.g., bowtie, Vivaldi, and wire helix. Despite its benefits, it suffers from a few disadvantages, e.g., the network mismatch when it is placed on the human body, as well as the large aperture at low microwave frequencies. The latter is of importance in diagnostic scans due to the penetration depth factor [20].

Besides, these limitations have meant that in practice, these antennas were of limited use for biomedical applications, due to bulky forms, large reflections, and mismatch. In this work, these disadvantages were successfully mitigated by embedding the antenna device inside a high-dielectric and low-conductive composite, with a permittivity close to that of the human skin (i.e., 40–45). Also, numerous materials were tested, e.g., solid (ceramics), liquid (oil and glycerol), semisolid (paraffin), and their mixtures [20–23]. In addition, water with a permittivity of 79 within the 1 GHz to 3 GHz range could not be used, due to high dielectric loss. Moreover, the mixture of the deionized filtered water and glycerol could not be utilized either, due to high energy absorption. The dielectric loss was not an issue with the oil, but the canola oil exhibited low-permittivity characteristics [23].

A composite of barium titanate ($BaTiO_3$) and titanium oxide (TiO_2) met the requirements with high permittivity and low conductivity. However, being a brittle ceramic, machining it into the complex structures (i.e., the proposed PDRH device) was exceedingly difficult. In order to address this challenge, other approaches based on employing composites to attain correct permittivity values were proposed. Consequently, the most promising case was the mixture of linseed oil and paraffin, which also simplified the production of the proposed ceramic material.

Lastly, the objective of this work was to realize a novel ceramic composite to develop a hybrid electromagnetic (EM) system, capable of measuring belly fat underneath the human skin (i.e., the subcutaneous or visceral fat), in order to effectively monitor the individual's health condition, using the deployed reflection method. The contributions of this work can be further summarized as:

(1) The high-dielectric and low-conductive composite materials were proposed and developed, such as VLF-440, TiO_2, and their mixtures, which can be used in the other monitoring systems when operating on the body, to miniaturize the device, and to further minimize the mismatch effects, and consequently, improving the overall EM performance.
(2) The skin-matched mixture of the 2 × VLF-440 and 1 × TiO_2 with the low conductivity factor was developed and its dielectric properties were measured within the operating range (i.e., 0.3–3.3 GHz). The latter is also selected for the systems that aim to monitor inside the body.
(3) The compact PDRH antenna was designed based on the full-wave finite integration technique (FIT) modeling, taking into account the measured properties of the skin-matched composite, to efficiently operate on the body in the frequency range of 0.9 GHz to 1.4 GHz, which further resulted in the improved range resolution and penetration depth.

The rest of the work is organized as follows. Section 2 covers the development of the proposed composites. Section 3 covers the design and evaluation of the proposed antenna device based on the hybrid EM design, modeling, and performance analysis. Section 4 concludes the paper.

2. Composite Materials Development and Characterization

A range of dielectric materials and their mixtures with high permittivity and low conductivity were considered for the intended biomedical application. Among the materials, barium titanate and neodymium titanate were of particular interest, due to their electrical properties being suitable for body-centric EM applications [20,24]. In this work, a commercial powder was carefully selected, i.e., VLF-440 by MRA Laboratories. This powder was produced for the production of small capacitors; thus, for the proposed application, much larger parts would be needed. This required the powder to be cold-pressed, and as the powder was not designed for this application, there was no guidance on how best to press the samples. Thus, further experimentation with the pressing force was required.

The cylindrical metal dies with diameters of 30 and 120 mm were then utilized. The preliminary experiments were performed with the smaller (metal) die, and the cold-pressing pressure of 3 MPa was found to be sufficient for the desired sample, as also indicated in Figure 1a. The procedure was conducted using the hand-powered hydraulic press, i.e., MTI YLJ-15. For the 120 mm metal die, the force required was much higher due to the large area; thus, the electrically-powered hydraulic press was utilized, i.e., Collin P300E. Moreover, due to the size of the samples, and the limited control over the press machines, two separate pressings were required. First, it was hot-pressed at 0.5 MPa at 180 °C, to compress the powder; hence, on the second pressing at 1.6 MPa, the press would have already taken the slack out of the system, and thus, would have given a repeatable applied pressure. A lower pressure was applied to the larger sample, as it was more fragile due to its higher aspect ratio. The burnout cycle in the furnace and the sintering cycle, were fully conducted on the powder, in order to efficiently densify the material, and to further prepare it for the next step.

The compressed sample as given in Figure 1b, was further sintered according to the procedure provided by the powder supplier, i.e., summarized in Table 1. In this regard, the samples were sintered using the Lenton UAF 15/27 furnace. Figure 2 depicts the shrinkage rate that was obtained based on the larger ceramic sample; i.e., shrank to 87 mm, as presented in Figure 1c. This sintered sample had a uniform structure, without any cracks or bends, which was further affirmation that the deployed pressing and sintering conditions were suitable, and were appropriately conducted. The density of the manufactured sample was also measured as 4.493 g per centimeter (g/cm).

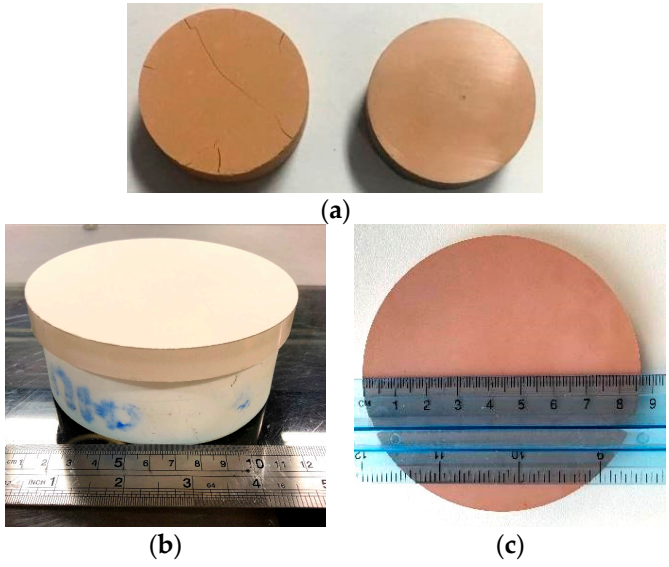

(**a**)

(**b**) (**c**)

Figure 1. The proposed and manufactured cylindrical composite ceramics: (**a**) the 30 mm samples (left: 4 tons). (**b**) The compressed 120 mm sample. (**c**) The sintered 87 mm sample.

Table 1. The temperature vs. time stages for the deployed sintering process.

(1) 20 to 300 °C at 0.1 °C/min	(2) 300 to 400 °C at 0.3 °C/min
(3) 400 to 985 °C at 10 °C/min	(4) 985 °C and hold for 5 h
(5) 985 to 20 °C at 5 °C/min	

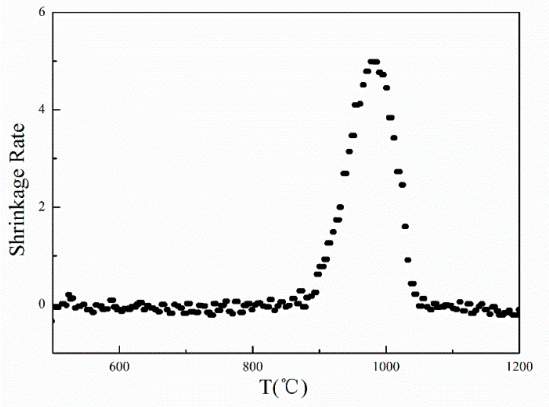

Figure 2. The shrinkage rate of the ceramic during the deployed sintering process.

While the conditions were suitable for producing the pure barium titanate, the permittivity of the pure material was not a perfect match for the skin. Besides, titanium oxide was chosen to blend with barium titanate, in order to increase the permittivity factor to the target value. The 99.5% pure rutile-TiO_2 (r-TiO_2) powder by Sigma-Aldrich Co. was then blended with $BaTiO_3$.

The selection of r-TiO_2 was due to its considerable dielectric properties (i.e., higher permittivity and lower conductivity), compared to the other types of TiO_2, for instance, anatase or brookite [23]. The r-TiO_2 was without the binder, therefore, to produce the pure sample, the pressureless furnace sintering could not be employed. Instead, the rutile was sintered using the FCT Systeme 25D spark plasma sintering furnace at 1100 °C, in the same conditions as commonly deployed [25,26].

To characterize the developed materials, the open-ended coaxial probe method was used, as it has been established as one of the core techniques for the dielectric measurements in this frequency range. In addition, the vector network analyzer (VNA), along with the electronic calibration module (ECal), as well as the dielectric probe, were fully employed to measure the electrical properties of the manufactured materials. Also, the setup shown in Figure 3 was calibrated with the distilled water, in order to improve the precision of the conducted EM measurements.

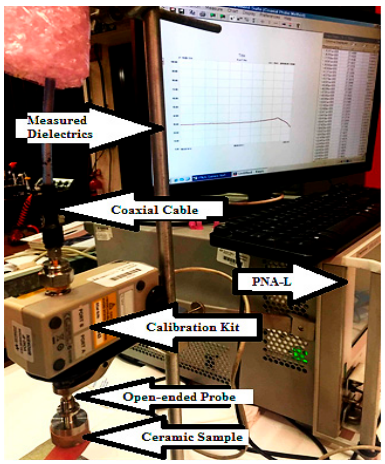

Figure 3. The arranged setup for the measurement of the electrical and dielectric properties of the proposed and manufactured ceramic composites, based on the open-ended coaxial probe method.

The open-ended probe method [27,28] was then applied to measure all types of ceramics, e.g., VLF-440, TiO_2, and their mixtures at the room temperature of 20 °C. The measurements were further validated using the cavity technique at 1.8 GHz. The target center frequency of 1 GHz was selected based on the tissue penetration capability, as well as the required bandwidth, in order to provide the desired high resolution. Figure 4 depicts the measured permittivity values of the human skin within the frequency range of 0.3–3.3 GHz, which was also considered as the reference. It is worth noting that the low-conductive materials have interesting properties, due to the lower absorption, and thus, the better penetration depth within the complex EM propagation medium [29,30].

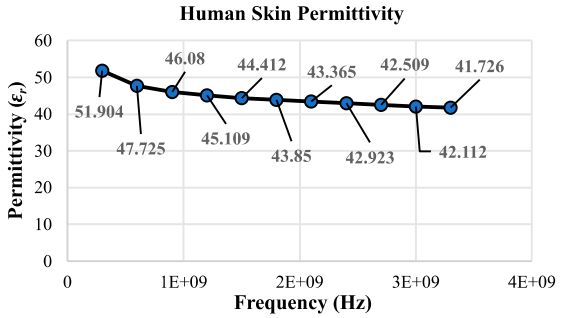

Figure 4. The human skin permittivity values at 0.3–3.3 GHz (in the base unit Hz), generated based on the available data reported in [29,30].

The permittivity and conductivity of VLF-440, TiO_2, and their mixtures, as measured using the discussed open-ended probe method, are shown in Figure 5a,b, respectively. The results at the target frequency of 1 GHz are given in Table 2 that shows that the composition of VLF-440 (2) + TiO_2 (1) was the closest to the skin permittivity values, and thus, was selected for the intended application. It should be noted that to evaluate the permittivity, the plot provided in Figure 4 was compared with the green plot in Figure 5a, to further elaborate on the subsequent EM-based system modeling.

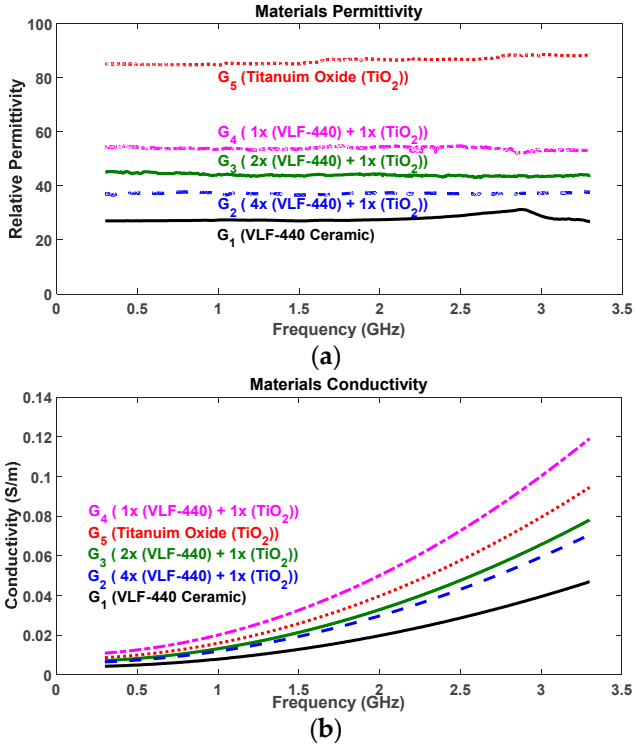

Figure 5. The measured electrical and dielectric properties of VLF-440, TiO_2, and their mixtures at 0.3–3.3 GHz: (**a**) the measured permittivity plots. (**b**) The measured conductivity plots.

Table 2. The measured dielectric properties of the proposed and manufactured composite materials, based on the open-ended coaxial probe method.

Dielectric Material	Frequency (GHz)	Relative Permittivity	Conductivity (S/m)
VLF-440	1.0	27.4	0.008
TiO_2	1.0	84.7	0.016
VLF-440 (1) + TiO_2 (1)	1.0	53.5	0.02
VLF-440 (4) + TiO_2 (1)	1.0	37.2	0.012
VLF-440 (2) + TiO_2 (1)	1.0	44.2	0.013

3. Antenna Design and Evaluation

The design and selection of the high-performance WB antenna played a vital role in measuring the abdominal fat, based on the concept of reflected pulses. This section comprehensively covers the design, EM modeling, and performance evaluation of the proposed microwave PDRH antenna.

3.1. Microwave Antenna Design and Analysis

As one of the targets of this work, the antenna device was proposed that was able to operate in the proximity of the human body. Due to the large reflections and size, as well as the permittivity mismatch among the complex mediums at the low microwave frequencies, the output characteristics differ from that of the free-space EM propagation that further results in the weak penetration effects. Therefore, a number of body-centric antennas and systems have been reported [31,32].

In this regard, the DRH antennas exhibit the desired output EM characteristics, such as the wide bandwidth, high gain, wide interference reduction, and matching capability. Yet, their fabrication, as well as their miniaturization, are considered as the major challenges for the practical implementation due to their bulky assemblies that limit their use for the body-centric applications. There have been several attempts in order to address the miniaturization aspects of these types of antennas [20].

Moreover, the antenna operates very effectively if the filling material is matched to the skin, for the systems that aim to monitor inside the human body. Hence, a closely-matched medium with the skin minimizes the reflection mismatch that is caused by a large difference in the permittivity, which also results in a large reflection, and consequently, reduced pulses through the body. Therefore, the proposed and manufactured skin-matched ceramic was used to design the intended PDRH antenna according to the standard dimensions [33]. Besides, the flare length, as well as the dimensions of the ridges, were computed to match the impedance. An antenna system in the free-space experiences an impedance of 377 ohms. Hence, if the antenna is built or immersed in another dielectric medium, the impedance should be computed accordingly [23]. Thus, the relative permittivity of the ceramic was further utilized for the size reduction, as well as for the effective elimination of reflections, as part of the hybrid EM design, modeling, and performance evaluation.

The realized medium for the antenna had a permittivity of 44.2 at 1 GHz, as provided in Table 2. Hence, the impedance of the medium can be obtained as 56.6 ohms, consequently resulting in a 6.6 times size reduction compared to the case of free-space propagation [34]. This process miniaturized the antenna at the desired frequency. Besides, the exponentially-tapered section was important, as it matched the reference impedance in the feeding point to that of the material at the aperture, which was varying from 50 ohms to 56.6 ohms.

Furthermore, Figure 6a,b depicts the dimensions for the accurate hybrid full-wave modeling. Figure 6c,d presents the dimensions of the embedded ceramic, designed based on the measured data from the fabricated mixture material that was loaded into the CST Studio Suite. This software was used to remove the minor errors introduced during the measurements based on performing the curve fitting techniques on the loaded data as in Figure 7. The mixture was further selected as the background material in the software, to effectively evaluate the dielectric medium. Additionally, the high-performance computing (HPC)-based full-wave simulations were conducted, using the robust time-domain transient solver. This hybrid numerical and experimental modeling were rigorously

performed, in order to evaluate the characteristics of the proposed system, and to further replicate the practical scenarios [35]. In addition, the main figures of merit, including the reflection coefficient (S_{11}), far-field radiation pattern, and gain were obtained, as depicted in Figure 8a–c, respectively. The S_{11} plot shows the wide bandwidth of 536 MHz, in the range of 0.91 GHz to 1.44 GHz, with −10 dB as the selected reference, along with the two large reflections at the low frequencies of 0.99 GHz and 1.29 GHz. Also, the far-field radiation patterns, as in Figure 8b, present the operation of the embedded ceramic antenna at both the largest reflection frequencies that exhibit promising directivity, when the device was placed on the body. Figure 8c also presents the high gain values for the proposed antenna over the frequency range of interest at two reflection points (i.e., 0.99 GHz = 7.7 dB and 1.29 = 9.4 dB). This result was successfully achieved by incorporating the low-conductive material into the performed hybrid modeling, which resulted in the significant shrunk size, as well as the improved matching.

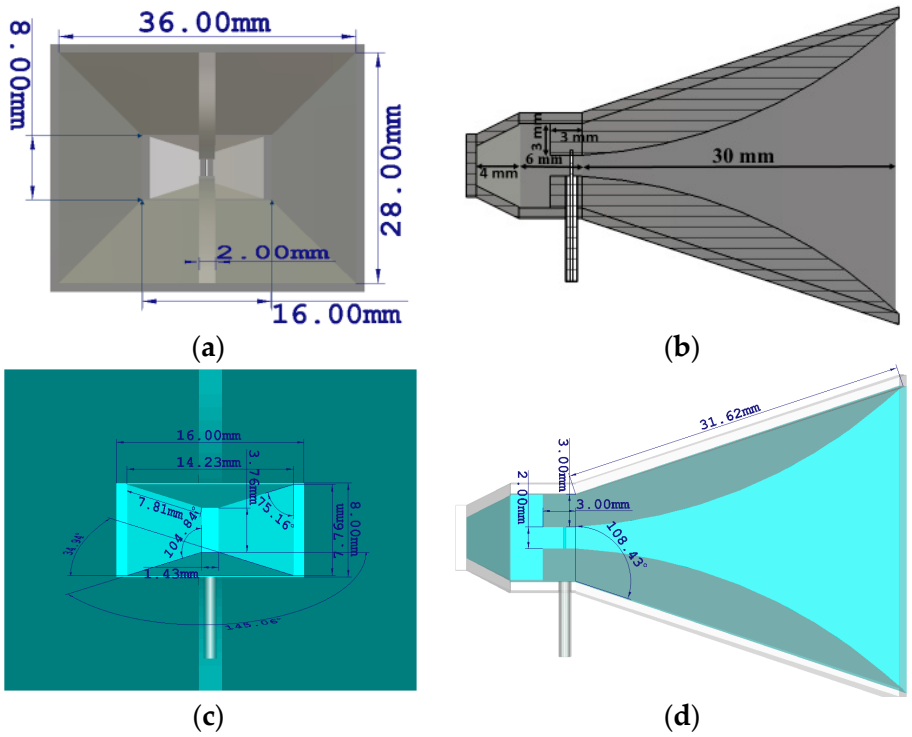

Figure 6. The structure and aperture dimensions of the proposed antenna device: (**a**) the front view. (**b**) The side view. (**c**) The back view of the embedded composite. (**d**) The side view of the embedded composite. It depicts the internal part that facilitates the EM propagation in the complex medium.

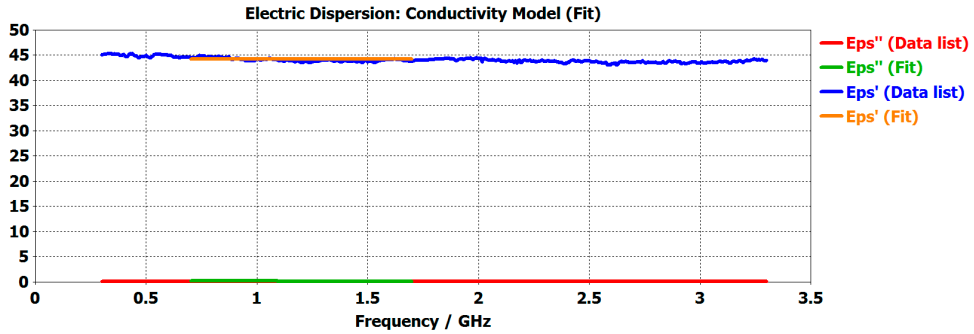

Figure 7. The measured electrical properties of the manufactured skin-matched ceramic composite, loaded into the CST software for the post-processing step, as part of the hybrid EM design.

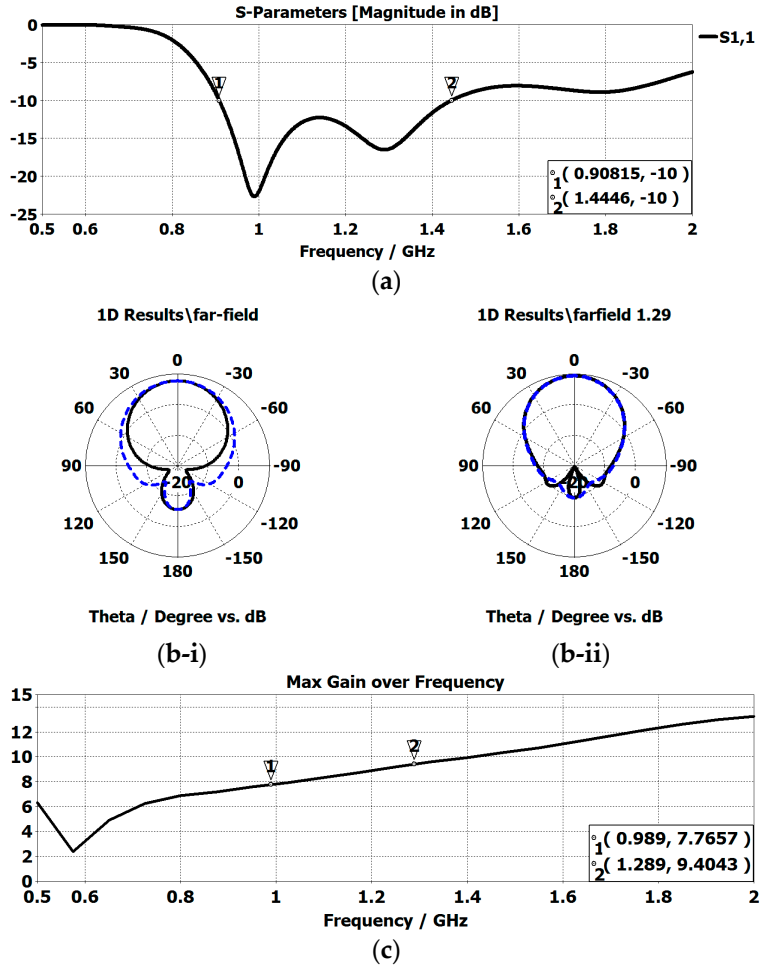

Figure 8. The output EM characteristics of the antenna system: (**a**) the S_{11} plot in the skin-matched dielectric medium, (**b-i**) the radiation patterns at 0.99 GHz with −13.5 dB sidelobe levels (SLLs). (**b-ii**) The radiation patterns at 1.29 GHz with −18.5 dB SLLs. (**c**) The maximum gain. It is worth noting the border between the near-field and far-field regions is indistinguishable for the monitoring purposes, due to the electrical properties of the developed microwave antenna device.

3.2. System Evaluation Using the Abdominal Tissue Model

The human arm model, consisting of two layers of 2 mm skin and infinite muscle, was defined based on the assumption that the pulse is absorbed within the muscle layer, as depicted in Figure 9a. In addition, the Gaussian pulse with the frequency and bandwidth of 1 GHz was then generated as a transmitted pulse, due to its penetration capability and high resolution. It should also be noted that the electrical properties of the tissue layers were imported from the database within the CST.

The arm model was created for the purpose of calibration and elimination of the effects of the skin and muscle tissues. The S_{11} plot shown in Figure 9b depicts a large reflection of −42.75 dB at the frequency of 0.93 GHz. Moreover, Figure 9c shows the transmitted and reflected pulses when the fat layer did not exist. It shows the highest time-framed reflected amplitude at 6.7 ns. This was obtained according to the expected time of arrival (provided in Table 3), along with the time for the incident pulse to be transmitted at its highest amplitude, i.e., 4 to 5 ns, which suggested that the time window should be selected at 6 ns to 7 ns. Besides, the next step was to model the abdomen tissue consisting of three layers (i.e., 2 mm skin, 15–30 mm fat, and infinite muscle), and further placing the antenna on this modeled tissue, as shown in Figure 10a. The fat thicknesses of the modeled tissue were changing from 15 mm to 30 mm with an iteration of 5 mm. The reflection of each case was then recorded, when the Gaussian pulse with the bandwidth of 500 MHz was transmitted into the tissue, as in Figure 10b.

The highest amplitude of the reflected pulse was also observed in the screening time window of 6 ns to 7 ns, which is the arrival window time of the reflected pulse. The thickness of the fat layer was changing from 15 mm to 30 mm, and the highest reflected points of the amplitude and time within the screening window (i.e., o1 to o5 shown in Figure 10b) were fully recorded for each reflection, and are given in Table 4. The S_{11} plots were obtained for these cases when the fat thicknesses were changing from 15 mm to 30 mm, which shows the relative changes in terms of the magnitude and frequency shift, as presented in Figure 10c. Table 4 was further employed to obtain the estimated equations for the amplitude change, and the time shift, when the thickness values were changing from 15 mm to 30 mm, as depicted in Figure 11a,b, respectively. The presented hybrid EM framework, as well as the generated closed-form analytical expressions, can be used to measure the abdominal fat, and to be further used in the different bioinstrumentation and biosensor components, designs, and applications.

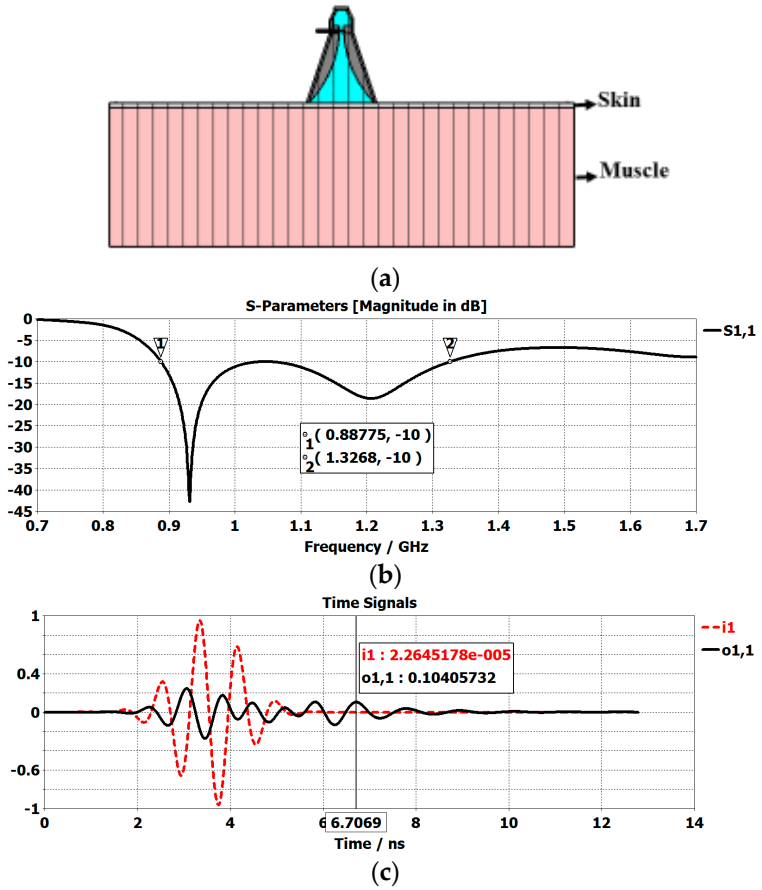

Figure 9. The hybrid modeling and output evaluations: (**a**) the modeled tissue without the fat layer. (**b**) The S_{11} plot when the fat layer did not exist. (**c**) The transmitted and reflected pulses into and back from the modeled tissue, for the retrieval of the highest amplitude.

Table 3. The traveling time for the pulse in the complex medium at 1 GHz, computed based on the parameters of the different environments.

Environment	Connector	Antenna	Tissue	Tissue
Material	Teflon	Ceramic	Skin	Fat
Permittivity	2.1	44	44	10
Length [l] (mm)	10	31	2.0	10
Velocity [v] (m/s)	207,019	452,267	452,267	948,683
Time [t] (ns)	0.096	1.371	0.088	0.211

Table 4. The time and magnitude differences at the first large reflection.

Fat Thickness (mm)	Time (ns)	Amplitude (v)
10	6.17	0.19
15	6.19	0.28
20	6.20	0.33
25	6.22	0.36
30	6.23	0.37

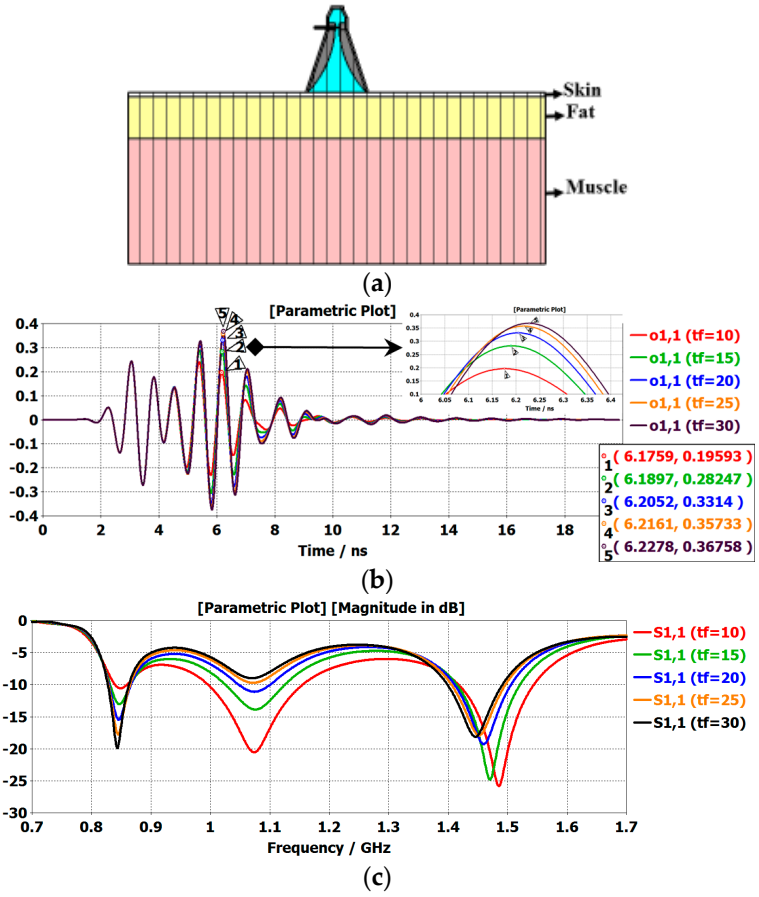

Figure 10. The output EM characteristics of the antenna system: (**a**) the modeled tissue with the fat layer. (**b**) The reflections of the pulses for the different fat thicknesses (i.e., 10–30 mm) with a 5 mm iteration. (**c**) The S_{11} plot when the fat thickness was changing from 10 to 30 mm.

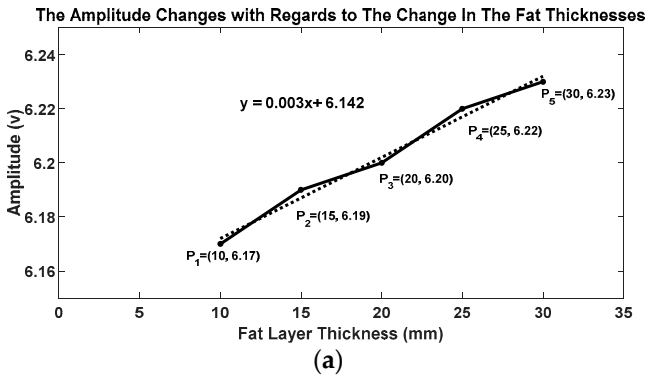

Figure 11. *Cont.*

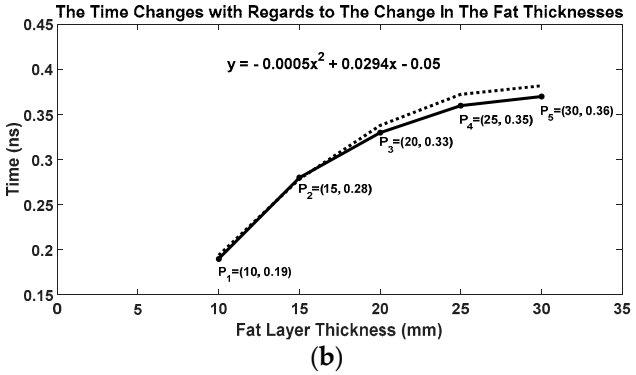

(**b**)

Figure 11. The graphs and equations generated based on the hybrid EM simulation data, in the first large reflection: (**a**) the rate of change in the amplitude. (**b**) The rate of change in the time.

4. Discussion and Conclusions

This work has validated the appropriateness of the proposed skin-matched composite for biomedical applications, as well as for the miniaturized antenna design with the required output EM characteristics when it was placed next to the body. As one of the primary objectives, improving the electrical and dielectric properties of the commercially available powder to that of the human skin could be successfully demonstrated. The developed ceramic was mixed homogeneously with TiO_2 in a number of portions, and was pressed, sintered, and the electrical properties were further obtained using the open-ended coaxial probe measurements. Besides, the antenna was redesigned using the properties of the skin-matched ceramic, based on the conducted full-wave hybrid EM modeling and performance evaluation. This stage not only improved the output characteristics when the antenna was placed on the tissue, but also significantly miniaturized it. In addition, the antenna was utilized to transmit the Gaussian pulse into the multilayer tissue, consisting of the skin, fat, and muscle. The mentioned steps were thoroughly conducted, to extract the amplitude and time factors of the signal reflections, to generate the graphs, and to further derive the closed-form mathematical expressions for the effective approximation of the thickness of the fat layer, using the deployed EM techniques.

In summary, the investigation has covered the development of the skin-matched high-dielectric ceramic that was utilized for the hybrid design and modeling of the PDRH antenna for the proposed body-centric application. The antenna filled with the high-dielectric composite exhibited promising outputs and figures of merit at the low microwave frequencies; e.g., the improved penetration, wide bandwidth, and higher resolution. Moreover, the equations obtained based on the hybrid modeling, and the deployed reflection methods were further utilized to determine the body fat thickness.

Furthermore, it should be noted that the works in [23,35] paved the way for the benchmarking of the deployed hybrid numerical and experimental EM modeling, through validating the obtained results and further depicting the agreement between the simulations and measurements. It should also be mentioned that the works in [23,35] resulted in the 3D-printed antenna devices that are very different from the antenna proposed in this work. This research has also resulted in the realization of a novel skin-matched composite, which was used in the hybrid design, to show its great potential to be used in biomedical applications. Those works were also based on the low-dielectric materials, along with different structures and EM properties, as opposed to this high-performance system. This antenna was not fabricated, to validate the feasibility of the hybrid framework. This was also due to the need for access to the laser cutting machine, which will be the subject of the next stage. Lastly, the core of this work was extracted from the Ph.D. thesis available in [36].

Author Contributions: Conceptualization, S.S., A.R., Y.A. and C.G.P.; Data curation, S.S. and A.R.; Formal analysis, S.S., A.R., Y.A., T.G.S., J.L. and C.G.P.; Investigation, S.S., A.R. and T.G.S.; Methodology, S.S., A.R., Y.A., T.G.S. and J.L.; Project administration, Y.A. and C.G.P.; Resources, Y.A. and C.G.P.; Software, S.S. and A.R.; Supervision, Y.A.; Validation, S.S., A.R., Y.A., T.G.S. and C.G.P.; Visualization, S.S. and A.R.; Writing—original draft, S.S. and A.R.; Writing—review & editing, S.S., A.R., Y.A., T.G.S., J.L. and C.G.P. All authors have read and agreed to the published version of the manuscript.

Funding: This research received no external funding.

Conflicts of Interest: The authors declare no conflict of interest.

References

1. Ford, N.D.; Patel, S.A.; Narayan, K.V. Obesity in Low- and Middle-Income Countries: Burden, Drivers, and Emerging Challenges. *Annu. Rev. Public Health* **2017**, *38*, 145–164. [CrossRef]
2. Canoy, D.; Boekholdt, S.M.; Wareham, N.; Luben, R.; Welch, A.; Bingham, S.; Buchan, I.; Day, N.; Khaw, K.-T. Body fat distribution and risk of coronary heart disease in men and women in the European Prospective Investigation into Cancer and Nutrition in Norfolk cohort: A population-based prospective study. *Circulation* **2007**, *116*, 2933–2943. [CrossRef]
3. Saito, Y.; Takahashi, O.; Arioka, H.; Kobayashi, D. Associations between body fat variability and later onset of cardiovascular disease risk factors. *PLoS ONE* **2017**, *12*, e0175057. [CrossRef] [PubMed]
4. De Pergola, G.; Silvestris, F. Obesity as a Major Risk Factor for Cancer. *J. Obes.* **2013**, *2013*, 291546. [CrossRef] [PubMed]
5. Mohammed, M.S.; Sendra, S.; Lloret, J.; Bosch, I. Systems and WBANs for Controlling Obesity. *J. Health Eng.* **2018**, *2018*, 1–21. [CrossRef] [PubMed]
6. Bray, G.A.; Heisel, W.E.; Afshin, A.; Jensen, M.D.; Dietz, W.H.; Long, M.; Kushner, R.F.; Daniels, S.R.; Wadden, T.A.; Tsai, A.G.; et al. The Science of Obesity Management: An Endocrine Society Scientific Statement. *Endocr. Rev.* **2018**, *39*, 79–132. [CrossRef]
7. Ramírez-Vélez, R.; Correa-Bautista, J.E.; Martínez-Torres, J.; Meneses-Echavez, J.F.; González-Ruíz, K.; González-Jiménez, E.; Schmidt-RioValle, J.; Lobelo, F. LMS tables for waist circumference and waist–height ratio in Colombian adults: Analysis of nationwide data 2010. *Eur. J. Clin. Nutr.* **2016**, *70*, 1189–1196. [CrossRef] [PubMed]
8. Staten, M.A.; Totty, W.G.; Kohrt, W.M. Original Investigations Measurement of Fat Distribution by Magnetic Resonance Imaging. *Investig. Radiol.* **1989**, *24*, 345–349. [CrossRef]
9. Omar, A.; Caverly, R.; Doherty, W.; Watkins, R.; Gopinath, A.; Vaughan, J.T. A Microwave Engineer's View of MRI. *IEEE Microw. Mag.* **2011**, *12*, 78–86. [CrossRef]
10. Caverly, R.H. RF Aspects of High-Field Magnetic Resonance Imaging (HF-MRI): Recent Advances. *IEEE J. Electromagn. RF Microwaves Med. Biol.* **2019**, *3*, 111–119. [CrossRef]
11. Yoshizumi, T.; Nakamura, T.; Yamane, M.; Islam, A.H.M.W.; Menju, M.; Yamasaki, K.; Arai, T.; Kotani, K.; Funahashi, T.; Yamashita, S.; et al. Abdominal Fat: Standardized Technique for Measurement at CT. *Radiology* **1999**, *211*, 283–286. [CrossRef]
12. Jensen, M.D.; Kanaley, J.A.; Reed, J.E.; Sheedy, P.F. Measurement of abdominal and visceral fat with computed tomography and dual-energy x-ray absorptiometry. *Am. J. Clin. Nutr.* **1995**, *61*, 274–278. [CrossRef]
13. Atta, H.R. *Ophthalmic Ultrasound: A Practical Guide*; Churchill Livingstone: Edinburgh, UK, 1996.
14. Kletsov, A.; Druchinin, S.; Khripkov, A.; Cho, J.; Chernokalov, A. Microwave non-contact imaging of subcutaneous human body tissues. *Health Technol. Lett.* **2015**, *2*, 108–111. [CrossRef]
15. Bahramiabarghouei, H.; Porter, E.; Santorelli, A.; Gosselin, B.; Popovic, M.; Rusch, L.A. Flexible 16 Antenna Array for Microwave Breast Cancer Detection. *IEEE Trans. Biomed. Eng.* **2015**, *62*, 2516–2525. [CrossRef]
16. Federal Communications Commission. *Revision of Part 15 of the Commission's Rules Regarding Ultra-Wideband Transmission Systems*; FCC-10-151; Federal Communications Commission: Washington, DC, USA, 2010.
17. Walton, K.; Sundberg, V. Broadband ridged horn design. *Microwave J.* **1964**, *4*, 96–101.
18. Bruns, C.; Leuchtmann, P.; Vahldieck, R. Analysis and simulation of a 1–18-GHz broadband double-ridged horn antenna. *IEEE Trans. Electromagn. Compat.* **2003**, *45*, 55–60. [CrossRef]
19. Cohn, S. Properties of Ridge Wave Guide. *Proc. IRE* **1947**, *35*, 783–788. [CrossRef]

20. Hilger, I.; Dahlke, K.; Rimkus, G.; Geyer, C.; Seifert, F.; Kosch, O.; Thiel, F.; Hein, M.; di Clemente, F.S.; Schwarz, U.; et al. ultraMEDIS–ultra-wideband sensing in medicine. In *Ultra-Wideband Radio Technologies for Communications, Localization and Sensor Applications*; IntechOpen: Rijeka, Croatia, 2013.
21. Latif, S.I.; Shafai, L.; Pistorius, S.; Flores-Tapia, D. Design and performance analysis of the miniaturised water-filled double-ridged horn antenna for active microwave imaging applications. *IET Microwaves Antennas Propag.* **2015**, *9*, 1173–1178. [CrossRef]
22. Latif, S.; Flores-Tapia, D.; Herrera, D.R.; Nepote, M.S.; Pistorius, S.; Shafai, L. A Directional Antenna in a Matching Liquid for Microwave Radar Imaging. *Int. J. Antennas Propag.* **2015**, *2015*, 751739. [CrossRef]
23. Sarjoghian, S.; Sagor, H.; Alfadhl, Y.; Chen, X. A 3D-Printed High-Dielectric Filled Elliptical Double-Ridged Horn Antenna for Biomedical Monitoring Applications. *IEEE Access* **2019**, *7*, 94977–94985. [CrossRef]
24. Yu, C.; Zeng, Y.; Yang, B.; Donnan, R.; Huang, J.; Xiong, Z.; Mahajan, A.; Shi, B.; Ye, H.; Binions, R.; et al. Titanium Dioxide Engineered for Near-dispersionless High Terahertz Permittivity and Ultra-low-loss. *Sci. Rep.* **2017**, *7*, 6639. [CrossRef]
25. Marinel, S.; Choi, D.H.; Heuguet, R.; Agrawal, D.; Lanagan, M. Broadband dielectric characterization of TiO_2 ceramics sintered through microwave and conventional processes. *Ceram. Int.* **2013**, *39*, 299–306. [CrossRef]
26. Wypych, A.; Bobowska, I.; Tracz, M.; Opasinska, A.; Kadlubowski, S.; Krzywania-Kaliszewska, A.; Grobelny, J.; Wojciechowski, P. Dielectric Properties and Characterisation of Titanium Dioxide Obtained by Different Chemistry Methods. *J. Nanomater.* **2014**, *2014*, 124814. [CrossRef]
27. Aimoto, A.; Matsumoto, T. Noninvasive method for measuring the electrical properties of deep tissues using an open-ended coaxial probe. *Med. Eng. Phys.* **1996**, *18*, 641–646. [CrossRef]
28. Alanen, E.; Lahtinen, T.; Nuutinen, J. Measurement of dielectric properties of subcutaneous fat with open-ended coaxial sensors. *Phys. Med. Biol.* **1998**, *43*, 475–485. [CrossRef]
29. Gabriel, S.; Lau, R.W.; Gabriel, C. The dielectric properties of biological tissues: III. Parametric models for the dielectric spectrum of tissues. *Phys. Med. Biol.* **1996**, *41*, 2271–2293. [CrossRef]
30. Ibrani, M.; Ahma, L.; Hamiti, E. The Age-Dependence of Microwave Dielectric Parameters of Biological Tissues. In *Microwave Materials Characterization*; IntechOpen: Rijeka, Croatia, 2012; pp. 139–158.
31. Li, X.; Jalilvand, M.; Sit, Y.L.; Zwick, T. A Compact Double-Layer On-Body Matched Bowtie Antenna for Medical Diagnosis. *IEEE Trans. Antennas Propag.* **2014**, *62*, 1808–1816. [CrossRef]
32. Nadir, H.; Gharzouni, A.; Martinod, E.; Feix, N.; Tantot, O.; Bertrand, V.; Rossignol, S.; Lalande, M. Small form factor UWB antenna integrating geopolymer dielectric material. *IET Microwaves Antennas Propag.* **2019**, *13*, 2146–2152. [CrossRef]
33. Balanis, A. *Antenna Theory: Analysis and Design*, 4th ed.; John Wiley & Sons, Inc.: Hoboken, NJ, USA, 2016.
34. Mallahzadeh, A.R.; Dastranj, A.A.; Hassani, H.R. A Novel Dual-Polarized Double-Ridged Horn Antenna for Wideband Applications. *Prog. Electromagn. Res. B* **2008**, *1*, 67–80. [CrossRef]
35. Sarjoghian, S.; Alfadhl, Y.; Chen, X.; Parini, C.G. A 3D-Printed High-Dielectric Materials-Filled Pyramidal Double-Ridged Horn Antenna for Abdominal Fat Measurement System. *IEEE Trans. Antennas Propag.* **2020**, 1. [CrossRef]
36. Sarjoghian, S. Design and evaluation of microwave antennas for abdominal fat measurement systems. Ph.D. Thesis, School of Electronic Engineering and Computer Science, Queen Mary, University of London, London, UK, 2019.